6th ECCOMAS Conference on Smart Structures and Materials
SMART2013
Politecnico di Torino, 24-26 June 2013
E. Carrera, F. Miglioretti and M. Petrolo (Editors)
www.smart2013.com

A COMPARATIVE STUDY OF SISO AND MIMO CONTROL STRATEGIES FOR FLOOR VIBRATION DAMPING

Iván M. Díaz[*], Emiliano Pereira[†], Carlos Zanuy[*], Cristina Alén[†]

[*] Universidad Politécnica de Madrid, Department of Continuum Mechanics and Theory of Structures
E.T.S. Ingenieros de Caminos, Canales y Puertos, 28040, Madrid, Spain
e-mail: ivan.munoz@upm.es, czs@caminos.upm.es, web page:
http://ingstruct.mecanica.upm.es

[†] Universidad de Alcalá de Henares, Department of Signal Theory and Communications
Escuela Politécnica Superior, 28805, Alcalá de Henares (Madrid), Spain
e-mail: emiliano.pereira@uah.es, cristia.alen@uah.es

Key words: Active vibration control, Inertial actuators, MIMO control, Human-induced vibrations, Floor vibrations.

Summary. *Civil engineering structures such as floor systems with open-plan layout or lightweight footbridges are susceptible to excessive level of vibrations caused by human loading. Active vibration control (AVC) via inertial mass actuators has been shown to be a viable technique to mitigate vibrations, allowing structures to satisfy vibration serviceability limits. Most of the AVC applications involve the use of SISO (single-input single-output) strategies based on collocated control. However, in the case of floor structures, in which most of the vibration modes are locally spatially distributed, SISO or multi-SISO strategies are quite inefficient. In this paper, a MIMO (multi-inputs multi-outputs) control in decentralised and centralised configuration is designed. The design process simultaneously finds the placement of multiple actuators and sensors and the output feedback gains. Additionally, actuator dynamics, actuator nonlinearities and frequency and time weightings are considered into the design process. Results with SISO and decentralised and centralised MIMO control (for a given number of actuators and sensors) are compared, showing the advantages of MIMO control for floor vibration control.*

1 INTRODUCTION

Improvements in design methods have led to light and slender floor structures with open-plan layouts. These floors satisfy ultimate limit state criteria but have the potential of attracting complaints coming from excessive human-induced vibrations [1]. Active vibration control (AVC) via inertial mass actuators has been shown to significantly reduce the level of response, allowing structures to satisfy vibration serviceability limits. Up to now, applications

mainly involve the use of SISO (single-input single-output) strategies based on collocated control (i.e., the pair actuator/sensor (A/S) are physically placed at the same point) rather than MIMO (multiple-inputs multiple-outputs) strategies. This is due to the fact that SISO control strategies are easier to be designed and, unconditional stability and good vibration reduction performance can be achieved under the absence of actuator and sensor dynamics [2]. Although the inclusion of actuator and sensor dynamics makes the stability conditional and degrades the vibration reduction performance, there exist SISO control strategies that mitigate these problems (see for example [3] and [4]).

Floor structures exhibits vibration modes which are usually locally spatially distributed with closely spaced natural frequencies. This means that there is no single location that can be used to control all the significant modes. Under these circumstances, several pairs of A/Ss should be used. The design should take into account the action of all the A/S pairs. However, such action can be considered in two different configuration: (i) if these pairs act independently of each other, this strategy is known as decentralised control, and (ii) if the actuator output takes into account not only its sensor partner but also all the others, this strategy is referred to as centralised control, or "full MIMO strategy". The main drawback associated to the use of decentralised control is that one can assure the control of one point but cannot assure the control at other points [5].

Generally speaking, MIMO control has the potential to achieve a better tradeoff between energy consumption and vibration reduction performance in the case of multiple vibration modes with natural frequencies closely spaced distributed. This statement was shown in [6], where an optimal placement of actuators and sensors for MIMO control of floor vibrations was presented. A two-stage algorithm, which combines a performance index (PI) and a time weighting function to consider the level and the duration of the vibration, was used to simultaneously find an optimal location of a predefined number of A/S pairs and the feedback gains of direct velocity feedback (DVF) control. The main conclusion is that a MIMO strategy control may be more appropriate than SISO and a decentralised MIMO control. In addition, the algorithm proposed in [6] considers the force/stroke saturation of the actuators and higher unmodelled modes of the floor, showing that a MIMO control is robust to this saturation and unmodelled floor dynamics.

This work builds on the idea of MIMO vibration control of floor structures, proposing an extension of the algorithm presented in [6]. The control strategy proposed is also based on DVC control, considering not only force/stroke saturation of the actuators and a time weighting function into the PI, but also the actuator dynamics, which affects significantly the stability of the overall control system. Then, a PI representative of the dissipation energy and obtained from an initial disturbance is minimised. Additionally, the human perception of vibrations depends on the magnitude, frequency content and duration of the vibration and the orientation of the body. Thus, the design of a control strategy should consider these factors. In this paper, the control strategy also includes a frequency weighting function which takes into account the dependency of the perception of vibration on the frequency [7].

The proposed design process is run assuming, firstly, SISO control, secondly, decentralised MIMO control, and, thirdly, centralised MIMO control, in order to carry out a comparative study between them. The study is undertaken for an all-side simply supported rectangular

plate which models a floor structure. The design process needs, as input, the structural modal model, which may be obtained analytically, if possible, by a finite element model or, experimentally, by an experimental modal testing. Finally, the advantages and disadvantages of each strategy are highlighted.

2 COMPONENTS OF THE CONTROL SCHEME

The general control strategy and the main elements of the control scheme are described below.

2.1 General control strategy

Figure 1 shows block diagram of a MIMO output feedback control in which the objective is to achieve zero vibration (reference command is set to zero $\underline{r}(t)=\underline{0}$). When the gain matrix *K* is diagonal, the control is decentralised and when it is a scalar number, the control is SISO. The floor and the actuation system have been represented using a state-space model [8]. The control scheme is completed by a saturation nonlinearity which limits the control voltage in order to avoid force and stroke saturation [9].

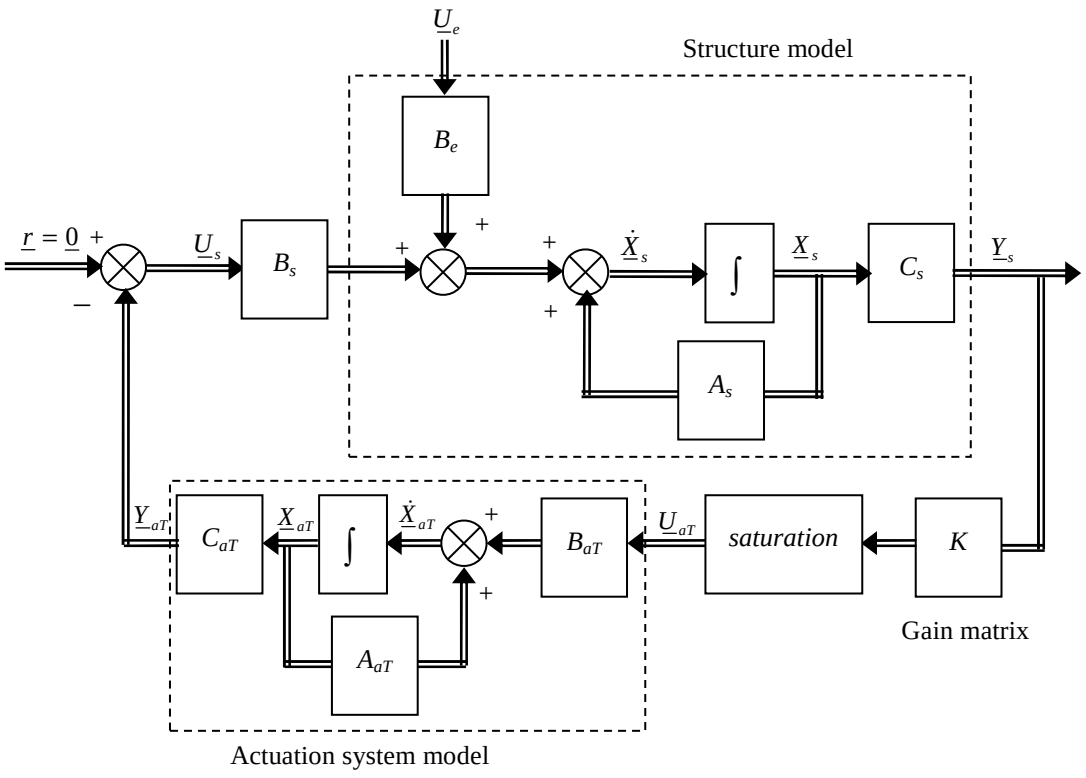

Figure 1: Control strategy using output feedback.

2.2 State-space model of the floor

A distributed parameter system (like a floor structure) can be discretised (using the finite element method) such that mass, damping and stiffness properties are lumped at *n* degrees of freedom. The dynamic behaviour is represented by *n*-coupled second-order differential equations that can be expressed in matrix form as

$$M\underline{\ddot{u}}(t)+D\underline{\dot{u}}(t)+K\underline{u}(t)=\underline{F}(t), \tag{1}$$

where $\underline{u}(t)=[u_1,u_2,\ldots,u_n]^T$ is the displacement vector, $\underline{F}(t)=[F_1,F_2,\ldots,F_n]^T$ is the force vector and *M*, *D* and $K\in\mathbb{R}^{n\times n}$ are the mass, damping and stiffness matrices. Using the modal analysis and the mode superposition method (or separation of variables), the displacement vector is expressed as a linear combination of a generalised coordinates (usually known as normal or modal coordinates) $\underline{\eta}(t)=[\eta_1,\ldots,\eta_m]^T$, *m* being the number of vibration modes considered into the analysis. That is,

$$\underline{u}(t)=\Phi\underline{\eta}(t), \tag{2}$$

where $\Phi\in\mathbb{R}^{n\times m}$ is the modal transformation matrix which contains the modal shapes in columns,

$$\Phi=\left[\underline{\phi}_1\ \ldots\ \underline{\phi}_m\right], \text{ with } \underline{\phi}_i\in\mathbb{R}^{n\times 1} \text{ and } i=1,\ldots,m. \tag{3}$$

Thus, $\underline{\phi}_i$ are the base vector and η_i are the coordinates of the modal model. The substitution of (2) into (1) and pre-multiplying by Φ^T yield a set of *m*-decoupled second-order differential equations. Its matrix representation considering mass-normalised mode shapes is as follows

$$I\underline{\ddot{\eta}}(t)+\Sigma\underline{\dot{\eta}}(t)+\Lambda\underline{\eta}(t)=\Phi^T\underline{F}(t), \tag{4}$$

where *I* is the identity matrix, $\Sigma=\mathrm{diag}(2\zeta_1\omega_1,\ldots,2\zeta_m\omega_m)$, $\Lambda=\mathrm{diag}(\omega_1^2,\ldots,\omega_m^2)$, $\Phi^T\underline{F}(t)$ are de modal participation factors, and ζ_i and ω_i are the damping ratio and natural frequency associated to the *i*-vibration mode.

Consider a state-space representation of (4) in which subscripts *s* and *e* indicates structure and excitation, respectively,

$$\underline{\dot{X}}_s(t)=A_s\underline{X}_s(t)+B_s\underline{U}_s(t)+B_e\underline{U}_e(t);\ \underline{Y}_s(t)=C_s\underline{X}_s(t), \tag{5}$$

in which the state vector is $\underline{X}_s=[\eta_1,\ldots,\eta_m,\dot{\eta}_1,\ldots,\dot{\eta}_m]^T$, the system matrix

$$A_s=\begin{bmatrix}0_{m\times m} & I_{m\times m}\\ -\Lambda & -\Sigma\end{bmatrix}, \tag{6}$$

the control input $\underline{U}_s = \left[F_{F1}, \ldots, F_{Fp} \right]^T$ for p actuators, the input matrix

$$B_s = \begin{bmatrix} 0_{m \times p} \\ \Phi_a \end{bmatrix}, \text{ with } \Phi_a = \begin{bmatrix} \phi_{1,F1} & \cdots & \phi_{1,Fp} \\ \vdots & \ddots & \vdots \\ \phi_{m,F1} & \cdots & \phi_{m,Fp} \end{bmatrix}, \tag{7}$$

where $\Phi_a \in \mathbb{R}^{m \times p}$ and $\phi_{i,Fj}$ is the value of the modal shape i at the position of the actuator j. The output vector is $\underline{Y}_s = \left[\dot{u}_{S1}, \ldots, \dot{u}_{Sq} \right]^T$, in which is assumed that the velocity is the quantity measured at q points. The output matrix is as follows

$$C_s = \begin{bmatrix} 0_{q \times m} \\ \Phi_s \end{bmatrix}, \text{ with } \Phi_s = \begin{bmatrix} \phi_{1,S1} & \cdots & \phi_{m,S1} \\ \vdots & \ddots & \vdots \\ \phi_{1,Sq} & \cdots & \phi_{m,Sq} \end{bmatrix}, \tag{8}$$

where $\Phi_s \in \mathbb{R}^{m \times q}$ and $\phi_{i,Sj}$ is the value of the modal shape i at the position of the sensor j. Finally, B_e is the system noise input matrix and $\underline{U}_e(t)$ is the system noise.

From the state-space representation (5), the characteristic equation is given by [8]

$$\left| \lambda_s I - A_s \right| = 0, \tag{9}$$

λ_s being the open-loop poles of the structure (or eigenvalues of A_s).

2.3 Actuator dynamic behaviour

The actuator considered is an inertial actuator that generates forces through acceleration of an inertial mass to the structure on which it is placed. The actuator consists of an inertial (or moving) mass m_a attached to a current-carrying coil moving in a magnetic field created by an array of permanent magnets. The inertial mass is connected to the frame by a suspension system. The mechanical part is modelled by a spring stiffness k_a and a viscous damping c_a. The electrical part is modelled by the resistance R, the inductance of the coil L and the voice coil constant C_e, which relates the coil velocity and the back electromotive force (Figure 2a) [10]. Combining the mechanical and the electrical part, the linear behaviour of the actuator can be closely described as a third-order dynamic model. As was shown in [11], the transfer function between the inertial force and the control voltage can be split into two parts: a second-order model (a mass-spring damper model) and a low-pass element (which represent the electrical part)

$$G_a(s) = \frac{F_a(s)}{V(s)} \left(\frac{g_a s^2}{s^2 + 2\zeta_a \omega_a s + \omega_a^2} \right) \left(\frac{1}{s + \varepsilon} \right), \tag{10}$$

where $s = j\omega$, ω being the angular frequency, $g_a > 0$, and ζ_a and ω_a are, respectively, the damping ratio and natural frequency. The pole at $-\varepsilon$ provides the low-pass property.

From Equation (10), the following state-space model can be obtained

$$\dot{\underline{X}}_a(t) = A_a \underline{X}_a(t) + B_a \underline{U}_a(t);\ \underline{Y}_a(t) = C_a \underline{X}_a(t), \tag{11}$$

in which the state vector is $\underline{X}_a = [x_1, x_2, x_3]^T$, the system, input and output matrices are

$$A_a = \begin{bmatrix} 0 & 0 & \varepsilon\omega_a \\ 1 & 0 & \omega_a^2 + 2\zeta_a\omega_a\varepsilon \\ 0 & 1 & \varepsilon + 2\zeta_a\omega_a \end{bmatrix},\ B_a = \begin{bmatrix} 0 \\ 0 \\ g_a \end{bmatrix} \text{ and } C_a = \begin{bmatrix} 0 & 0 & 1 \end{bmatrix}, \tag{12}$$

respectively. The control input $\underline{U}_a = V \in \mathbb{R}$ is the control voltage for the actuator and the output is the transmitted force to the structure $\underline{Y}_a = F_a \in \mathbb{R}$.

The state-space model (11) for one actuator can be generalised for *p* actuators quite straightforwardly. Thus, the state-space model for the total number of actuators is as follows (it was referred as the actuation system in Figure 1)

$$\dot{\underline{X}}_{aT}(t) = A_{aT} \underline{X}_{aT}(t) + B_{aT} \underline{U}_{aT}(t);\ \underline{Y}_{aT}(t) = C_{aT} \underline{X}_{aT}(t), \tag{13}$$

in which the model matrices are

$$A_{aT} = \begin{bmatrix} A_{a1} & 0 & \cdots & 0 \\ 0 & A_{a2} & \cdots & 0 \\ \vdots & \vdots & \ddots & \vdots \\ 0 & 0 & 0 & A_{ap} \end{bmatrix},\ A_{aT} \in \mathbb{R}^{3p \times 3p},\ B_{aT} = \begin{bmatrix} B_{a1} & 0 & \cdots & 0 \\ 0 & B_{a2} & \cdots & 0 \\ \vdots & \vdots & \ddots & \vdots \\ 0 & 0 & 0 & B_{ap} \end{bmatrix},\ B_{aT} \in \mathbb{R}^{3p \times p}$$

$$\text{and, } C_{aT} = \begin{bmatrix} C_{a1} & 0 & \cdots & 0 \\ 0 & C_{a2} & \cdots & 0 \\ \vdots & \vdots & \ddots & \vdots \\ 0 & 0 & 0 & C_{ap} \end{bmatrix},\ C_{aT} \in \mathbb{R}^{p \times 3p}. \tag{14}$$

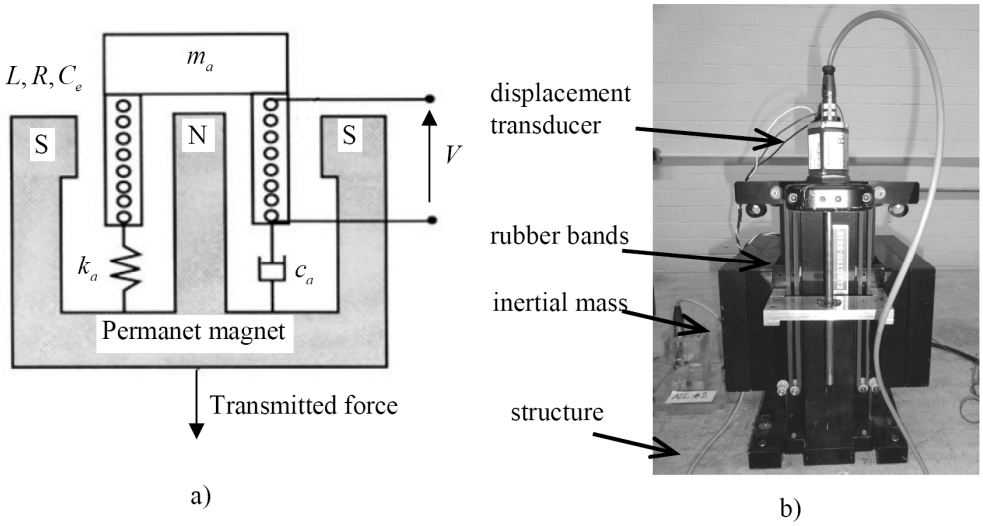

Figure 2: Inertial actuator. a) Sketch of an electrodynamic actuator (after [10]). b) APS Electro-Seis Dynamic Shaker 400.

2.4 Frequency weighting

The vibration that can be perceived by a human depends on the direction of incidence to the human body and the frequency content of the vibration (for a given amplitude), among other factors. As such, the variation of sensitivity of frequency for a body position can be taken into account by attenuating or enhancing the system response for frequencies where perception is less or higher sensitive, respectively. The degree to which the response is attenuated or enhanced is referred to as frequency weighting. Thus, frequency weighting functions are applied in order to account for the different acceptability of vibrations for different directions and body positions. ISO 2631 [7] and BS 6841 [12] provide details for frequency and direction weighting functions that can be applied which are all based on the baricentric coordinate system shown in Figure 3. These have been included in current floor design guidelines such as the SCI guidance [13]. According to ISO 2631, for z-axis vibration and standing and seating, the frequency weighting function is W_k. This curve and its asymptotic definition are graphed in Figure 4. Thus, the frequency weighted state vector is obtained as follows in frequency domain

$$\underline{X}_{s,w}(s) = \underline{X}_s(s) \cdot W_k(s), \tag{15}$$

in which $W_k(s)$ is the transfer function (or Fourier transform) of the frequency weighting function. Equation (15) can also be expressed in time domain as

$$\underline{X}_{s,w}(t) = \underline{X}_s(t) * w_k(t), \tag{16}$$

where $(*)$ denotes the convolution process and $w_k(t)$ is the impulse response function of $W_k(s)$.

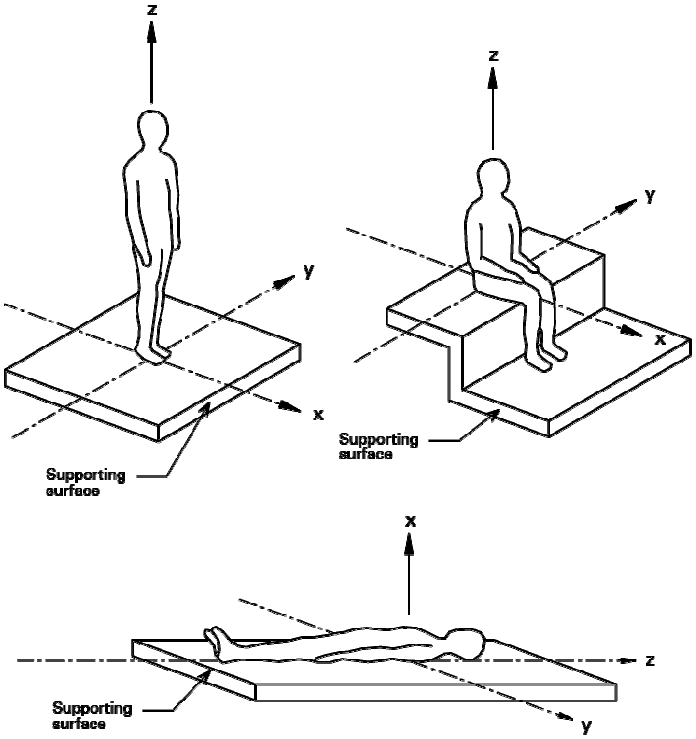

Figure 3: Directions for vibration according to ISO 2631 [7] and BS 6841 [12] (after [13]).

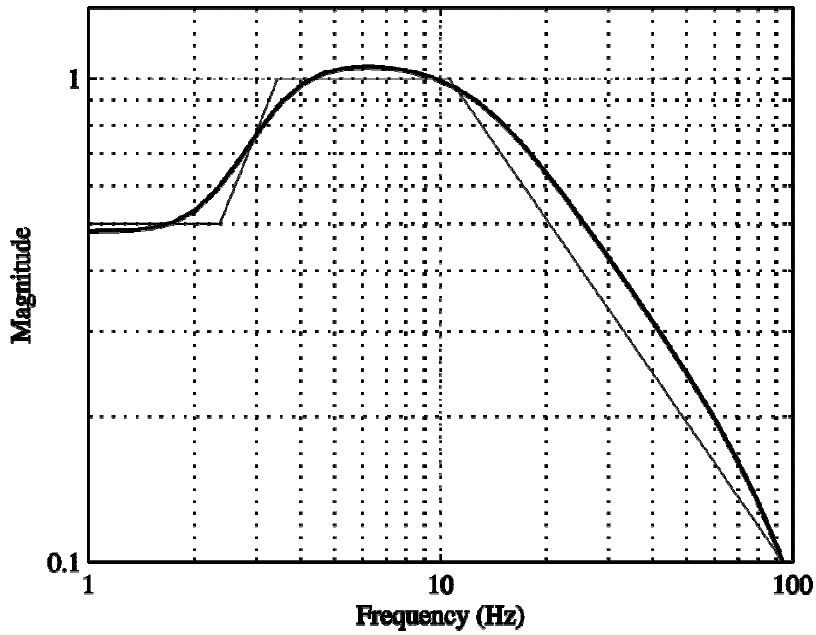

Figure 4: W_k frequency weighting function (thicker curve) and its asymptotic definition (thinner curve) [7].

2.5 Time weighting

As it has been mentioned before, the human comfort to vibration is directly related to the duration of sustained vibration. Thus, persistent vibrations should be penalised in the control design, giving more importance to transient vibration of long-duration than those of short-duration. As it was commented before, the control design proposed in this work consists of minimizing a PI that depends on the energy of the system after an initial condition. Therefore, exponential time weighting will be suitable for this application. The time weighted state $\hat{\underline{X}}_s$ is computed from the state vector $\underline{X}_s$ as follows

$$\hat{\underline{X}}_s(t) = e^{\alpha t} \cdot \underline{X}_s(t). \tag{17}$$

with $\alpha \geq 0$. Note that the exponential time weighting adds a constraint in the relative stability of the controlled system. Note also that persistent states are more penalised as α is increased. Finally, if the state vector is time weighted by (17) and frequency weighted by (16), the time and frequency weighted state is as follows

$$\hat{\underline{X}}_{s,w}(t) = \hat{\underline{X}}_s(t) * w_k(t). \tag{18}$$

3 CONTROL DESIGN

The purpose of this section is to provide a procedure to find an optimal location of a given number of A/S pairs and the gain matrix when DVF of Figure 1 is considered.

3.1 Closed-loop system

Consider the floor model given by (5) in which is assumed the same number of actuators and sensors ($p = q$ in Equation (5)) located at the same point (in pairs). That is, p A/S pairs are considered. On the one hand, the control force ($\underline{U}_s(t)$ in Figure 1 and Equation (5)), which is the input to the structure and the output of the actuation system, can be expressed as follows

$$\underline{U}_s(t) = -\underline{Y}_{aT}(t) = -C_{aT}\underline{X}_{aT}(t). \tag{19}$$

Note that the saturation nonlinearity is omitted at this point. Substituting (19) into (5), it is obtained

$$\dot{\underline{X}}_s(t) = A_s\underline{X}_s(t) + B_s\left(-C_{aT}\underline{X}_{aT}\right) + B_e\underline{U}_e(t). \tag{20}$$

On the other hand, the control voltage, which is the input to the actuation system, is

$$\underline{U}_{aT}(t) = -K\underline{Y}_s(t) = -KC_s\underline{X}_s(t). \tag{21}$$

Substituting (21) into (11)

$$\dot{\underline{X}}_{aT}(t) = A_{aT}\underline{X}_{aT}(t) + B_{aT}KC_s\underline{X}_s(t). \tag{22}$$

Hence, the state-space model of the closed-loop system can be written using (20) and (22) as follows

$$\begin{bmatrix} \dot{\underline{X}}_s(t) \\ \dot{\underline{X}}_{aT}(t) \end{bmatrix} = \begin{bmatrix} A_s & -B_sC_{aT} \\ B_{aT}KC_s & A_{aT} \end{bmatrix} \begin{bmatrix} \underline{X}_s(t) \\ \underline{X}_{aT}(t) \end{bmatrix} + \begin{bmatrix} B_e \\ 0 \end{bmatrix} \underline{U}_e(t),\ \underline{Y}_s(t) = \begin{bmatrix} C_s & 0 \end{bmatrix} \begin{bmatrix} \underline{X}_s(t) \\ \underline{X}_{aT}(t) \end{bmatrix} \tag{23}$$

with the closed-loop system matrix being

$$A_c = \begin{bmatrix} A_s & -B_sC_{aT} \\ B_{aT}KC_s & A_{aT} \end{bmatrix}. \tag{24}$$

The characteristic equation of the closed-loop system is then [8]

$$\left|\lambda_c I - A_c\right| = 0, \tag{25}$$

λ_c being the closed-loop poles (or eigenvalues of A_c). The closed-loop system will be asymptotically stable if the real part of the ($2m$+$3p$) eigenvalues of A_c is negative

$$\mathrm{Re}\left(\lambda_{c,i}\right) < 0,\ \forall i = 1,\ldots,\left(2m+3p\right). \tag{26}$$

3.2 Design process

The design process is based on the minimisation of a PI related to the dissipation energy of the whole structure due to the AVC action for a given excitation. The PI is calculated using the time and frequency weighted structure states as follows (see Equation (18) and Figure 5)

$$J\left(K,\underline{Z}\right) = \frac{1}{2}\int_0^{t_f} \hat{\underline{X}}_{s,w}^T(t) Q \hat{\underline{X}}_{s,w}(t), \tag{27}$$

in which the weighting matrix $Q \in \mathbb{R}^{2m\times 2m}$ is a positive define matrix, $\underline{Z} \in \mathbb{R}^p$ is the position of the A/S pairs (obviously, $\underline{Z}$ must be included into the spatial domain of the structure) and t_f is the final time used to compute the PI. This time should be sufficiently long such that the system energy is totally dissipated due to the control action. The weighting matrix is taken as [6]

$$Q=\begin{bmatrix} \omega_1^2\phi_{1,\max}^2 & 0 & \cdots & 0 \\ 0 & \ddots & & \\ & & \omega_m^2\phi_{m,\max}^2 & \ddots & \vdots \\ \vdots & & \ddots & \phi_{1,\max}^2 & \\ & & & & \ddots & 0 \\ 0 & & \cdots & & 0 & \phi_{m,\max}^2 \end{bmatrix}, \tag{28}$$

in which $\phi_{i,\max}$ is the maximum value of the *i*-th eigenvector $\underline{\phi}_i$. Note that the displacement states are weighted by the natural frequencies, making thus the displacement states comparable to the velocity states. Figure 5 shows a block diagram which drafts the computation of the time and frequency weighted states used to obtain the PI (27). Note that the saturation nonlinearity is taken into account to compute the PI.

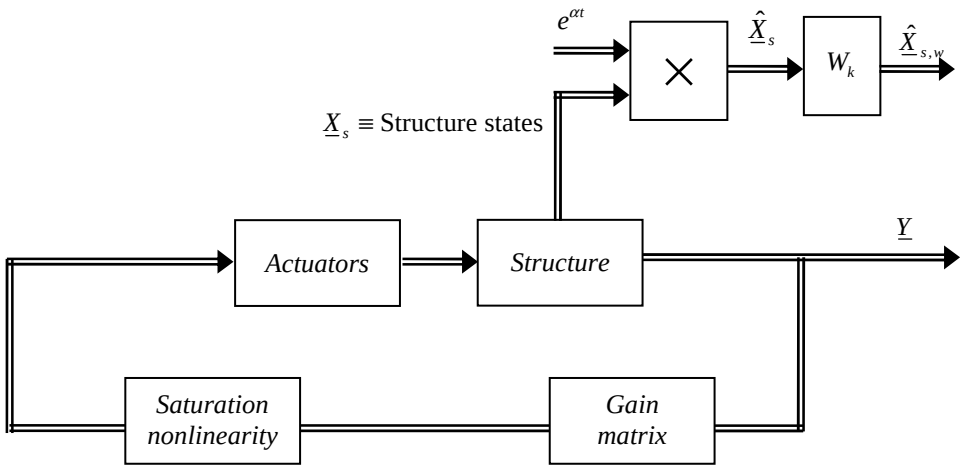

Figure 5: Block diagram of the computation of the PI.

The design process proposed for the A/S pairs location and the gain matrix can be divided into the following steps:

Step 1: Obtain a model of the structure considering *m* vibration modes defined at *n* points spatially distributed along the structure.

Step 2: Obtain the eigenvalues of open-loop structure (Equation (9)), choose parameter α as

$$\alpha \le \min_i \left|\mathrm{Re}\left(\lambda_{s,i}\right)\right|, \ \forall i = 1,\ldots,2m, \tag{29}$$

choose the final time used to compute the PI as

$$t_f \geq 10/\alpha, \tag{30}$$

decide the frequency weighting function to be used [7], the number of A/S pairs, *p*, and the excitation. Typically an initial condition for the structure states will be considered as perturbation.

Step 3: For each possible combination of positions of the *p* A/S pairs, find the optimal gain matrix *K* by minimising the PI (27) subjected to the stability condition for the closed-loop system shown in (26), but updated for exponentially weighted states. Mathematically, the problem may be established as

$$J\left(\underline{Z}\right) = \min_{K} J\left(K, \underline{Z}\right), \quad \text{s.t.} \quad \text{Re}\left(\lambda_{c,i}\right) < -\alpha, \ \forall i = 1, \ldots, 2m. \tag{31}$$

Step 4: When the optimal matrix gain for each possible combination of A/S pairs position is obtained, the combination of positions $\underline{Z}^*$, together with its corresponding gain matrix, that provides the minimum PI is the solution searched

$$J^* = \min_{\underline{Z}} J\left(\underline{Z}\right). \tag{32}$$

4 EXAMPLE

The study is undertaken for an all-side simply supported rectangular isotropic plate of dimension 10×6 m and a depth of 0.20 m. The material properties considered are: modulus of elasticity $E = 20 \times 10^9 \, N/m^2$, Poisson's ratio $\nu = 0.15$ and density $\rho = 3000 \, kg/m^3$. The density has been increased from $2500 \, kg/m^3$ (the characteristic value for reinforced or prestressed concrete) to $3000 \, kg/m^3$ in order to include a portion of the imposed load and the total dead load [13]. Figure 6 shows the spatial grid considered and the obtained natural frequencies and mode shapes. The damping ratio for all the modes has been taken as 0.02. This value is representative of partially fully fitted out floors. Note that the structure model can be obtained experimentally, through experimental modal analysis, or numerically, through the finite element method. Current experimental modal identification procedures use a state-space realisation, such as [14]. For the particular example considered here, the structure has analytical solution, which is not available for most real-life structures.

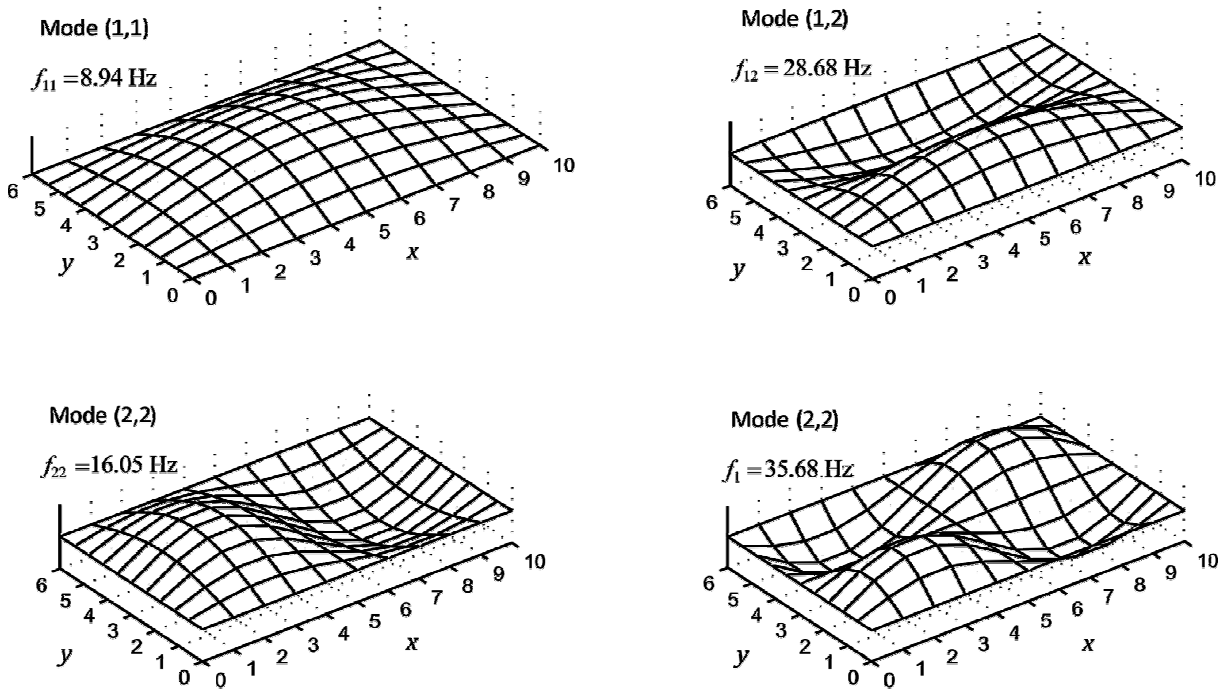

Figure 6: Grid and Mode shapes.

An APS Dynamics Model 400 electrodynamic shaker [15] operated in inertial mode with an inertial mass of 30.4 kg is considered here as the actuator (Figure 2a). The transfer function (10) was identified using voltage-driven mode as

$$G_a(s) = \frac{12000s^2}{s^3 + 60.32s^2 + 795.9s + 8204}, \tag{33}$$

in which $\omega_a = 13.2$ rad (2.1 Hz), $\zeta_a = 0.5$ and $\varepsilon = 47.1$.

The structure has been modelled considering the first four vibration modes ($m = 4$). The condition for α is obtained from (29): $\alpha \leq 1.12$. A value of $\alpha = 1.1$ was finally chosen. Using α, it is obtained the minimum time considered to compute the PI (Equation (30)): $t_f \geq 10/\alpha = 8.33$. A value of $t_f = 10$ s was decided to be used.

An impulsive input modelled via an initial condition of velocity structure states was used to disturbance the structure

$$\begin{bmatrix} \underline{X}_s(0) \\ \underline{X}_{aT}(0) \end{bmatrix} = \begin{bmatrix} \underline{X}_s(0) \\ 0 \end{bmatrix}, \text{ with } \underline{X}_s(0) = \left[\eta_1 = 0, \ldots, \eta_m = 0, \dot{\eta}_1 = 1, \ldots, \dot{\eta}_m = 1\right]^T. \tag{34}$$

Once all the needed parameters are selected, Steps 3 and 4 can be undertaken. Thus, the algorithm has been run for three cases: (1) only one A/S is considered ($p = q = 1$), (2) two A/S pairs ($p = q = 2$) in a decentralised configuration (the gain matrix is diagonal), and (3)

two A/S pairs ($p = q = 2$) in a centralised configuration (the gain matrix is a full matrix). For each case, the effect of the inclusion of the actuator is studied and the effect of frequency weighting is also studied.

Table 1 shows the PI obtained for the three cases considering two cases for each one: (i) the actuator behaves as constant (its dynamics and the saturation nonlinearity are not included), and (ii) the actuator dynamics and the saturation nonlinearity are included into the control scheme. Table 1 has been carried out considering time weighted states only. For the case of an ideal actuator, the transfer function of the actuator (10) is simplified as

$$G_a(s) \simeq \frac{g_a}{\varepsilon} = 241 \text{ N/V} . \tag{35}$$

Table 1 shows the PI value, the optimal position and the gain matrix components. For the ideal case, the PIs are much smaller than those obtained for the non-ideal case. The gain values are drastically reduced and the PIs are substantially increased for the non-ideal case mainly due to stability reasons.

Table 2 shows the PI obtained for the three cases considering two cases for each one: (i) time weighted states, and (ii) time and frequency weighted states. Table 2 has been carried out considering the actuator dynamics and the saturation nonlinearity.

From both tables, it is observed that MIMO control always provides smaller PIs than SISO control and that centralised MIMO always improves the performance of decentralised MIMO, although such improvement may not be very significant in this example.

	Ideal Actuator			Non-ideal Actuator		
	1 A/S	2 dec. A/Ss	2 cen. A/Ss	1 A/S	2 dec. A/Ss	2 cen. A/Ss
PI	$190 \cdot 10^{-6}$	$12.9 \cdot 10^{-6}$	$9.9 \cdot 10^{-6}$	$76.99 \cdot 10^{-4}$	$42.95 \cdot 10^{-4}$	$42.91 \cdot 10^{-4}$
Position (x,y)	(3.0,1.8)	(4.0,2.4) (3.0,1.8)	(3.0,1.8) (1.0,0.6)	(7.0,3.6)	(6.0,4,2) (7.0,1.8)	(6.0,4.2) (7.0,1.8)
K_{11}	$5.34 \cdot 10^{4}$	$2.52 \cdot 10^{4}$	$18.7 \cdot 10^{4}$	24.95	9.72	9.73
K_{22}	—	$6.00 \cdot 10^{4}$	$44.6 \cdot 10^{4}$	—	22.10	22.08
K_{12}	—	—	$-24.5 \cdot 10^{4}$	—	—	3.31

Table 1: PI including non-ideal actuator.

	Without Weighting			With Weighting		
	1 A/S	2 dec. A/Ss	2 cen. A/Ss	1 A/S	2 dec. A/Ss	2 cen. A/Ss
PI	$76.99 \cdot 10^{-4}$	$42.95 \cdot 10^{-4}$	$42.91 \cdot 10^{-4}$	$29.62 \cdot 10^{-4}$	$17.05 \cdot 10^{-4}$	$16.89 \cdot 10^{-4}$
Position	(7.0,3.6)	(6.0,4.2) (7.0,1.8)	(6.0,4.2) (7.0,1.8)	(5.0,2.4)	(4.0,1.8) (6.0,3.6)	(6.0,1.8) (5.0,4.8)
K_{11}	24.95	9.72	9.73	12.41	10.56	15.68
K_{22}	—	22.10	22.08		11.18	15.81
K_{12}	—	—	3.31		—	4.84

Table 2: PI including the frequency weighting function.

5 CONCLUSIONS

This paper presents the design of a MIMO strategy for controlling human-induced vibration on a floor structure. The design process consists of determining the position of A/S pairs and the control gains within a velocity feedback scheme. The design process considers: (i) time and frequency weighting for the states, which are used to compute the PIs, (ii) a PI, which is representative of the dissipation energy, is minimised, and (iii) the actuator dynamic behaviour is included. The inclusion of the actuator dynamics leads to more realistic results than those obtained in [6]. Additionally, the study carried out has shown the influence of frequency weighting into the design process. It has been demonstrated through the PI that MIMO control improves results with respect to SISO control and that centralised MIMO behaves better than decentralised MIMO. Table 3 gathers the pros and cons of the use of centralised control with respect to decentralised control.

This study will contribute to motivate future research on MIMO control for floor vibrations. Interesting topics susceptible to be explored are: optimal placement of inertial actuators within a MIMO control, more efficient (usually more complicated) control laws than the DVF control used here, environmental and economic assessment of the AVC and experimental implementation on in-service floors, among others.

Advantages	Disadvantages
Each actuator considers the vibration of the whole system	More complicated to be design
Non-transference of energy	Less intuitive design
Always improves results	

Table 3: Advantages and disadvantages of centralised versus discentralised control.

REFERENCES

[1] A. Ebrahimpour and R. L. Sack. A review of vibration serviceability criteria for floor structures. *Computers and Structures* 83, 2488–2494, 2005.

[2] M. J. Hudson and P. Reynolds. Implementation considerations for active vibration control in the design of floor structures. *Engineering Structures* 44, 334–358, 2012.

[3] I. M. Díaz, E. Pereira and P. Reynolds. Integral resonant control scheme for cancelling human-induced vibrations in light-weight pedestrian structures. *Structural Control and Health Monitoring* 19, 55–69, 2012.

[4] I. M. Díaz, E. Pereira, M. J. Hudson and P. Reynolds. Enhancing active vibration control of pedestrian structures using inertial actuators with local feedback control. *Engineering Structures* 41, 157–166, 2012.

[5] M. J. Hudson, P. Reynolds and D. Nyawako. Efficient design of floor structures using active vibration control. *ASCE Structures Congress* 401 (35), 2011.

[6] L. M. Hanagan, E. C. Kulasekere, K. S. Walgama and K. Premaratne. Optimal placement of actuators and sensors for floor vibration control. *Journal of Structural Engineering* 126(12), 1380–1387, 2000.

[7] ISO 2631-1. Mechanical vibrations and shock – evaluation of human exposure to whole-body vibration. Part 1. General requirement. International Organization for Standardization, 1997.

[8] R. S. Burns. *Advanced Control Engineering*. Butterworth-Heinemann, 2001.

[9] I. M. Díaz and P. Reynolds. On-off nonlinear active control of floor vibrations. *Mechanical Systems and Signal Processing* 24, 1711–1726, 2010.

[10] A. Preumont. Vibration Control of Active Structures: An Introuduction. Kluwer Academic Publishers, 2002.

[11] I. M. Díaz and P. Reynolds. Acceleration feedback control of human-induced floor vibrations. Engineering Structures 32(1), 163–173, 2010.

[12] BS 6841. Guide to measurement and evaluation of human exposure to whole-body mechanical vibration and repeated shock. *British Standards Institute*, 1997.

[13] A. L. Smith, S. J. Hicks, and P. J. Devine. Design of floors for vibration: A new approach (P354). *The Steel Construction Institute*, 2007.

[14] F. J. Cara, J. Capio, J. Juan and E. Alarcón. An approach to operational modal analysis using the expectation maximization algorithm. *Mechanical Systems and Signal Processing* 31, 109–129, 2012.

[15] APS Manual 400. Instruction Manual Electro-Seis Model 400 Shaker. APS Dynamics, INC., 2007.